Pergamon

Chemical Engineering Science, Vol. 50, No. 19, pp. 3033–3041, 1995

0009-2509/95 $9.50 + 0.00

0009-2509(95)00135-2

NUMERICAL SIMULATION OF A SIMULATED COUNTERCURRENT MOVING BED CHROMATOGRAPHIC REACTOR

AJAY K. RAY‡ and ROBERT W. CARR†
Department of Chemical Engineering and Materials Science, University of Minnesota, Minneapolis, MN 55455, U.S.A.

(*First received* 9 *November* 1994; *revised manuscript received and accepted* 4 *April* 1995)

Abstract—A mathematical model of a simulated countercurrent moving bed chromatographic reactor (SCMCR) has been developed. The model represents a multiple column reactor consisting of a series of either four or five tubular fixed beds packed with a mixture of catalyst and adsorbent, with a port that can serve either as an inlet or an outlet between each. A reversible first order reaction, $A \rightleftharpoons B$, with rate coefficients and rate parameters taken from the hydrogenation of 1, 3, 5-trimethylbenzene is incorporated into the model. The partial differential equations governing the isothermal reactor at 463 K are solved by an adaptive finite element method with uneven grid points. Model predictions of concentration profiles in the columns, and overall reactor performance, are obtained. It is shown that reaction and separation occur simultaneously, and that the conversion of this equilibrium limited reaction is greatly increased over the 0.62 that would be the maximum obtainable in a non-separative system. Under appropriate operating conditions, the model calculations predict that high product purity streams (98–99%) and nearly unit conversions can be obtained.

INTRODUCTION

A model of a simulated countercurrent moving bed chromatographic reactor (SCMCR), in which a reversible first-order heterogeneous reaction takes place on catalyst particles, is developed. In order to preserve the advantages of countercurrent operation while avoiding the problems associated with movement of solids that exists in true countercurrent moving beds, a simulated moving bed which employs a series of fixed beds with feed ports and product withdrawal ports located at the top and bottom of each bed is considered. The continuous countercurrent contact is simulated by successively switching feed and take-off streams from one inlet to the next in order to achieve relative movement between the feed and the bed. It is observed that reaction and separation can be achieved simultaneously and that the conversion of the equilibrium-limited reaction is greatly improved. Indeed, the variables and operating parameters that control the configuration of the reactor and its overall performance can be tailored so as to exceed the performance of a fixed bed both in yield and product purity.

In the equilibrium stage model previously reported (Ray *et al.*, 1994) it was assumed that concentrations are uniform in each stage so that the governing partial differential equations can be reduced to a system of ordinary differential equations. The configuration was a single fixed bed which was divided into a number segments with provision of adding feed to the stream passing from one segment to the next or of withdrawing a stream emerging from any segment.

In this paper, a model of a differently configured SCMCR has been developed. The multiple column configuration consists of a series of fixed beds (columns) connected by short lengths of empty tubing. Each column corresponds to a section of the single fixed bed above. An appropriate sequence of column switching can be designed to simulate a countercurrent flow system. Analysis of this configuration will be helpful since it is the most convenient configuration for laboratory experimental studies. The partial differential equations governing the reactor behavior are solved by a finite element method.

Along with its importance for reactor design and for simulation of countercurrent operation, the analysis and numerical solution of the mathematical model constitutes by itself an interesting and challenging problem. This can be seen by recognizing that the concentration profiles inside the reactor become transient upon each switch of feed position, requiring a transient model. Furthermore, the concentration fronts that propagate through the columns require a numerical procedure capable of resolving their shape. The method of finite elements constitutes a very attractive candidate for the numerical solution of the problem. This method combines the rapid convergence of the finite element method with the convenience associated with locating grid points or elements where the solution is important or has large gradients.

† Corresponding author.
‡ Present address: Department of Chemical Engineering, University of Groningen, Netherlands

MATHEMATICAL FORMULATION OF THE MODEL

The reactor is schematically represented in Fig. 1. Feed enters a particular column for a fixed length of time and then is switched to the next column. Carrier gas also enters a particular column, usually one column behind the feed column. Reactant and product are withdrawn from a specified column which must be changed simultaneously with the feed point advancement. When the feed point has progressed to the end of the sequence of columns, it is returned to the starting position and the process is repeated. The shifting of the feed and product positions in the direction of fluid flow simulates the movement of solids in the opposite direction.

The reactor consists of a number of columns of uniform cross section, each of length L and packed with a mixture of adsorbent and catalyst to a uniform void fraction ε through which carrier gas moves with speed u_g. The catalyst and adsorbent particle diameters are small enough that interparticle and intraparticle heat and mass transfer are unimportant. The dilution by carrier gas is sufficient to permit an isothermal treatment. Pressure drop in the relatively short columns is neglected, as is axial dispersion.

The adsorption-reaction system is described by the mechanism of eq. (1).

$$A(g) \underset{k_{dA}}{\overset{k_{aA}}{\rightleftharpoons}} A_{ads} \underset{k_b}{\overset{k_f}{\rightleftharpoons}} B_{ads} \underset{k_{dB}}{\overset{k_{aB}}{\rightleftharpoons}} B(g). \tag{1}$$

The model is formulated below for Langmuir adsorption isotherms, but this is relaxed to linear isotherms in the calculations since the reactant and product are highly diluted with carrier gas. Since the kinetics are first order, a linear model is obtained. Component B is less strongly adsorbed than component A and no distinction is made between adsorption on the catalyst or the adsorbent.

The one-dimensional material balance equation for both components in the fluid phase of a column is given by

$$\varepsilon \frac{\partial C_i}{\partial t} + \varepsilon u_g \frac{\partial C_i}{\partial X} = -(1-\varepsilon)k_{ai}(N - n_A - n_B)C_i + (1-\varepsilon)k_{di}n_i \tag{2}$$

and for the solid phase by

$$\frac{\partial n_i}{\partial t} = k_{ai}(N - n_A - n_B)C_i - k_{di}n_i - \alpha_i(k_f n_A - k_b n_B) \tag{3}$$

where $i = A$ (reactant) or B (product); $\alpha_A = -1$, $\alpha_B = 1$. The concentration in the fluid and solid phases are denoted by C and n. N is the limiting concentration of adsorbates on the solid surface. k_{ai} and k_{di} are the adsorption and desorption rate coefficients, and k_f and k_b are the forward and backward reaction rate coefficients. The transient terms in the equations must be retained to describe the concentration fronts that propagate through the columns each time the feed point is switched to a new feed column.

Two key parameters are the switching period, t_s, the time interval between successive advancements of the feed point, and the switching speed, ζ, the hypothetical or pseudo-linear flow rate of the solid phase. The switching period may conveniently be used as a characteristic time for the system. A dimensionless time can be defined as $\tau = t/t_s$, and the feed and take-off ports are advanced when $\tau = 1, 2, 3, \ldots$. The switching speed can be defined as the ratio of the length of a column to the switching period, eq. (4)

$$\zeta = \frac{L}{t_s}. \tag{4}$$

The parameter $\sigma = [(1-\varepsilon)/\varepsilon]\, NK\, u_s/u_g$, which plays a key role in the CMCR (Petroulas, 1984), has a counterpart for the SCMCR defined by

$$\sigma_i = \frac{1-\varepsilon}{\varepsilon} N_{\text{limiting adsorbate}} K_{\text{equilibrium},i} \frac{\zeta}{u_g} \tag{5}$$

in which the solids speed u_s is replaced by the pseudo-speed ζ.

Separation can be accomplished in the reactor by adjusting the carrier gas and pseudo-solid velocities, u_g and ζ, such that $\sigma < 1$ for one component and $\sigma > 1$ for the other. If $\sigma < 1$, that component will move more slowly than the feed point, and if $\sigma > 1$, it will move ahead of the feed point. Therefore, if the

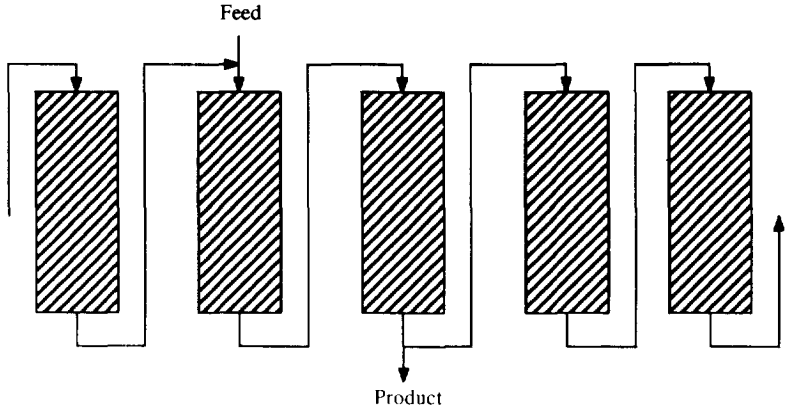

Fig. 1. Schematic diagram of multiple column differential model.

reactant A is made to travel behind the feedpoint, ($\sigma < 1$) its residence time, and hence the conversion, will increase. If, at the same time, the product B is made to travel ahead of the feed point, separation between A and B can be achieved and an improved product purity can be obtained. An observer located at the feed point will observe countercurrent separation of components A and B. Note that the adsorption equilibrium constants for each, K_i, must differ in order to obtain separation. Since the product has the smaller adsorption equilibrium constant, the relative adsorptivity, K, is greater than 1.

The variables have been made dimensionless as follows

$$\gamma_i = K_i C_i; \qquad \upsilon_i = \frac{n_i}{N}; \qquad \xi = \frac{X}{L};$$

$$K_i = \frac{k_{ai}}{k_{di}}; \qquad K_r = \frac{k_f}{k_b}; \qquad K = \frac{K_A}{K_B} \tag{6}$$

$$\mu_i = \frac{1-\varepsilon}{\varepsilon} N K_i; \qquad \lambda_i = \mu_i k_{di} t_s;$$

$$\delta_i = \mu_i k_f t_s; \qquad \beta = \frac{\zeta}{u_g}.$$

If adsorption–desorption equilibrium is attained at all times then the Langmuir isotherm, in the dimensionless variables we have chosen, takes the simple form

$$\upsilon_i = \frac{\gamma_i}{1 + \gamma_A + \gamma_B} = \frac{\gamma_i}{\Delta}, \quad \text{where } \Delta = 1 + \gamma_A + \gamma_B. \tag{7}$$

Equations (2) and (3) can then be written as

$$\frac{\partial \gamma_i}{\partial \tau} = -\frac{1}{\beta}\frac{\partial \gamma_i}{\partial \xi} - F_i \tag{8}$$

$$\mu_i \frac{\partial \upsilon_i}{\partial \tau} = F_i - R_i \tag{9}$$

where

$$F_i(\gamma_i, \upsilon_i) = \lambda_i[(1 - \upsilon_A - \upsilon_B)\gamma_i - \upsilon_i] \tag{10}$$

and

$$R_i(\upsilon_i) = \alpha_i \delta_i \left(\upsilon_A - \frac{\upsilon_B}{K_r}\right) \tag{11}$$

where $i = A$ (reactant) or B (product); $0 \leqslant \xi \leqslant 1$ for each column; and $\tau = 0, 1, 2, \ldots$ A switching in feed is performed whenever the characteristic time $\tau = 1, 2, 3, \ldots$

Adding eqs (8) and (9), the overall material balance can be written

$$\frac{\partial}{\partial \tau}(\gamma_i + \mu_i \upsilon_i) = -\frac{1}{\beta}\frac{\partial \gamma_i}{\partial \xi} - R_i. \tag{12}$$

If the reactor is operated with dilute mixtures of reactant in carrier gas, where the adsorption isotherm is approximately linear, $\Delta = 1$ and from eq. (7) we have $\upsilon_i = \gamma_i$. Then eq. (12), the overall material balance, reduces to

$$(1 + \mu_i)\frac{\partial \gamma_i}{\partial \tau} = -\frac{1}{\beta}\frac{\partial \gamma_i}{\partial \xi} - R_i. \tag{13}$$

For component A, eq. (13) can be written as

$$(1 + \mu_A)\frac{\partial \gamma_A}{\partial \tau} = -\frac{1}{\beta}\frac{\partial \gamma_A}{\partial \xi} + \delta_A \gamma_A - \frac{\delta_A}{K_r}\gamma_B \tag{14}$$

and for component B, it can be written as

$$(1 + \mu_i)\frac{\partial \gamma_B}{\partial \tau} = -\frac{1}{\beta}\frac{\partial \gamma_B}{\partial \xi} + \frac{\delta_B}{K_r}\gamma_B - \delta_B \gamma_A. \tag{15}$$

FINITE ELEMENT FORMULATION

In the Galerkin finite element approach (Strang and Fix, 1973; Finlayson, 1980) one looks for an approximate solution $\gamma(\xi, \tau)$ to an equation

$$L\gamma(\xi, \tau) = f \tag{16}$$

by setting the residual of the equation orthogonal to a set of basis functions

$$\int R\varphi_i \, d\xi = \int (L\gamma - f)\varphi_i \, d\xi = 0; \quad i = 1, 2, 3, \ldots, M. \tag{17}$$

Therefore, eq. (14) reduces to

$$(1 + \mu_A)\int_0^1 \frac{\partial \gamma_A}{\partial \tau}\varphi_i \, d\xi = -\frac{1}{\beta}\int_0^1 \frac{\partial \gamma_A}{\partial \xi}\varphi_i \, d\xi + \delta_A \int_0^1 \gamma_A \varphi_i \, d\xi - \frac{\delta_A}{K_r}\int_0^1 \gamma_B \varphi_i \, d\xi \tag{18}$$

The variable $\gamma_A(\xi, \tau)$ is expanded as a summation of a set of linearly independent finite element basis functions, φ_j, each multiplied by an unknown coefficient, γ_{Aj}, of the basis functions

$$\gamma_A = \sum_{j=1}^{M} \gamma_{Aj}\varphi_j. \tag{19}$$

In this work the basis functions are Hermite cubics. Then by inserting eq. (19) into eq. (18), we obtain eq. (20).

$$(1 + \mu_A)\sum_{j=1}^{M}\frac{\partial \gamma_{Aj}}{\partial \tau}\left(\int_0^1 \varphi_i \varphi_j \, d\xi\right) = -\frac{1}{\beta}\sum_{j=1}^{M}\gamma_{Aj}\left(\int_0^1 \varphi_i \frac{\partial \varphi_j}{\partial \xi} d\xi\right) + \delta_A \sum_{j=1}^{M}\gamma_{Aj}\left(\int_0^1 \varphi_i \varphi_j \, d\xi\right) - \frac{\delta_A}{K_r}\left(\int_0^1 \gamma_{Bi}\varphi_i \, d\xi\right) \tag{20}$$

where $i = 1, 2, 3, \ldots, M$.

The partitioning of the computational domain into discrete subdomains reduces a partial differential equation into a discrete set of M algebraic equations. In contrast to conventional finite element analysis, where domain tessellation remains fixed as a parameter is incremented or a time step is taken, the adaptive method used here moves or deforms the finite element tessellation at each time step or set of

parameter values, so that localized steep gradients and high curvatures can be resolved as they develop.

In the method used in the formulation (Finlayson, 1980; Davis and Flaherty, 1987; Benner *et al.*, 1987) both nodal amplitudes and nodal positions move continuously with time in such a way as to satisfy simultaneous differential equations which minimize the residuals. In this approach, the nodes generally move to those regions where they are most needed in order for the residuals resulting from the numerical approximations are zero at the nodal points.

Equation (20) can be rearranged to

$$(1+\mu_A)\sum_{j=1}^{M}\left(\int_0^1 \varphi_i\varphi_j\,d\xi\right)\frac{\partial\gamma_{Aj}}{\partial\tau} = \sum_{j=1}^{M}\left(-\frac{1}{\beta}\int_0^1 \varphi_i\frac{\partial\varphi_j}{\partial\xi}d\xi + \delta_A\int_0^1\varphi_i\varphi_j\,d\xi\right)\gamma_{Aj} - \frac{\delta_A}{K_r}\left(\int_0^1\gamma_{Bi}\varphi_i\,d\xi\right) \quad (21)$$

where $i = 1,2,\ldots,M$. The above equation is of the form of

$$\mathbf{U}\frac{\partial\gamma_A}{\partial\tau} = \mathbf{V}\gamma_A + \mathbf{F} \quad (22)$$

where

$$\mathbf{U} = (1+\mu_A)\sum_{j=1}^{M}\left(\int_0^1\varphi_i\varphi_j\,d\xi\right) \quad (23)$$

$$\mathbf{V} = \sum_{j=1}^{M}\left(-\frac{1}{\beta}\int_0^1\varphi_i\frac{\partial\varphi_j}{\partial\xi}d\xi + \delta_A\int_0^1\varphi_i\varphi_j\,d\xi\right) \quad (24)$$

and

$$\mathbf{F} = \frac{\delta_A}{K_r}\left(\int_0^1\gamma_{Bi}\varphi_i\,d\xi\right) \quad (25)$$

$\mathbf{U}$ and $\mathbf{V}$ are $(M\times M)$ matrices, and $\mathbf{F}$ is a $(M\times 1)$ vector. Equation (22) can be rearranged to

$$\frac{\partial\gamma_A}{\partial\tau} = \mathbf{U}^{-1}\mathbf{V}\gamma_A - \mathbf{U}^{-1}\mathbf{F}$$

$$\frac{\partial\gamma_A}{\partial\tau} = \mathbf{S}\gamma_A - \mathbf{T};\quad \gamma_A(0) = \gamma_{A0}. \quad (26)$$

The initial value problem is solved by the fourth-order Runge–Kutta method. For Hermite cubic basis functions, within a given element 16 integrations need to be performed for the stiffness matrix, $\mathbf{V}$, and mass or damping matrix, $\mathbf{U}$, and four integrations for the load vector or forcing function, $\mathbf{F}$. Since each function spans two adjacent elements, the global stiffness matrix will have a bandwidth of seven. The integrations were performed numerically using 3-points Gauss quadrature.

NONUNIFORM GRID BY ADAPTIVE FINITE ELEMENT METHODS OF EQUIDISTRIBUTION OF ERROR

The goal of an adaptive finite element method (Gelinas *et al.*, 1981; Davis and Flaherty, 1987; Benner *et al.*, 1987) is an optimal or nearly optimal set of nodal positions at each time step or set of parameter values, or both. Optimal means that the solution error is, in some sense, minimized. The adaptive techniques used here are based on an error bound that is independent of eq. (16). Strang and Fix (1973) used an error bound for the finite element representation (19) of $\gamma(\xi,\tau)$ with polynomials $\varphi_i(\xi)$ or order m:

$$e_i \leqslant Ch^m\int_{\xi_i}^{\xi_{i+1}}\left|\frac{d^{m+1}\gamma}{d\xi^{m+1}}\right|d\xi;\quad i = 1,2,\ldots,M \quad (27)$$

where C is a constant, h is mesh size $= \Delta\xi_i$; ξ_i is the position of the ith node.

Local error can be reduced by equidistribution of solution error among the elements. A set of equidistribution residuals R of eq. (27) can be defined:

$$R = e_i - e_0 = 0;\quad i = 1,2,\ldots,(M-1) \quad (28)$$

where e_0 is equidistribution error.

RESULTS AND DISCUSSION

Numerical simulations of the SCMCR were carried out using input parameters for the hydrogenation of 1,3,5-trimethylbenzene (MES) to 1,3,5-trimethylcyclohexane (TMC) in excess H_2 (25% v/v in N_2) at 463 K for comparison with previous investigations of this reaction in a countercurrent moving bed reactor (Fish and Carr, 1989), and in simulated countercurrency (Ray *et al.*, 1994; Ray and Carr, 1995). At 463 K Egan and Buss (1959) reported the reaction equilibrium constant to be 128. Also, the adsorption equilibrium constant for MES on alumina (4.84) and the adsorption equilibrium constant ratio for MES and TMC on alumina ($K/K = 4.0$) have been reported (Petroulas, 1984). The adsorption rate constants for MES and TMC were each estimated to be 200 cm/s. With the excess of hydrogen, the kinetics are pseudo-first order, making eq. (1) an appropriate representation of the kinetics.

To avoid the concentration discontinuities (shocks) that would be predicted within the columns by the one dimension dispersionless model, and thereby to avoid divergence of the computations, the following factors were incorporated. Hermite polynomials were used as basis functions so that both the concentration and the concentration gradient are continuous between finite elements. Also, only 15% of the total flow was collected as product so that large changes in flow rate do not occur, and with the added benefit that at periodic steady state the reactant concentration fronts are smoothed. Moreover, the non-uniform adaptive finite element mesh is used so that a large number of grid points can be present where significant concentration gradients exist.

Even with these modifications, we have had difficulties in terms of convergence of the numerical solution when working with non-linear models, so the calculations reported here will be restricted to linear models. Since the experiments with which we wish to make comparisons were done with dilute gaseous

solutions of reactants, where the adsorption isotherm is approximately linear, this restriction is not serious. Under the assumption that the solid and fluid phase concentrations are related by a linear adsorption isotherm, relatively simple solutions can be constructed for the model equations. Although the results that are obtained in this case are strictly valid only when the fluid stream is dilute this is just the case we are interested in, since experimental data for MES hydrogenation, dilute in N_2 carrier gas in a five-column SCMCR is available. Furthermore, the analysis and numerical simulation that can be performed in the linear case are quite important because of the insight that can be gained for the solution of the more complicated, non-linear problems.

Concentration profiles for the reactant and product within the columns were obtained from the solution of eq. (26). For each time step eqs (17) and (28) were solved for the coefficients γ_{Aj} (or γ_{Bj}), optimal node locations ξ_i and error constant e_0. The nodal positions ξ_i which approximately satisfy eq. (28) are computed after each continuation step or time step, but before Newton iteration for the nodal values of γ_{Aj} (or γ_{Bj}). This strategy preserves normal bandwidth of the stiffness matrix in the solution and eliminates non-linear phenomena that arise from nodal movement, thereby preserving the quadratic rate of convergence of Newton iteration. The discretized equations (17), which generally are non-linear and are solved by the Newton–Raphson iteration, are given by

$$\sum_{j=1}^{M} \frac{\partial R_i}{\partial \gamma_j} \Delta\gamma_j^{(k)} = -R_i; \quad i = 1, 2, \ldots, M \qquad (29)$$

where $\gamma^{(k)}$ is the kth iterate and $\Delta\gamma^{(k)} = \gamma^{(k+1)} - \gamma^{(k)}$ the kth update of γ for that time step. The Newton–Raphson method approaches quadratic convergence near a solution so long as the Jacobian is non-singular, i.e. its determinant is non-zero. The integrals in eq. (17) are evaluated by the isoparametric transformation of the subdomain of φ_i onto a subdomain of unit size, followed by Gaussian quadrature. The equations were solved by using 20 adaptive finite elements in each column with Hermite cubic basis functions. The dimensionless time step. $\Delta\tau$, used for the calculation was 0.0001.

Figure 2 shows the calculated concentration profiles within columns of a four-column configuration just at the end of a switching period. In the figure, the reactant is entering column 1, and the outlet stream from column 1 passes into column 2. Fifteen per cent of the exit stream from column 2 is collected as product, and the rest is sent to column 3. The outlet of column 4 enters column 1 along with 15% make up feed to replace withdrawn product. Concentration profiles were obtained for the mesitylene hydrogenation reaction with the reaction rate coefficients used to calculate concentration profiles in the single column equilibrium stage model (Ray *et al.*, 1994). The dotted line in the figures represents the reactant and the solid line represents the product. It can be seen that the product stream withdrawn from column 2 is highly enriched in the reaction product, trimethylcyclohexane.

The reactor works under transient conditions because of the periodic feed switching that is imposed on the system. However, a periodic steady state with

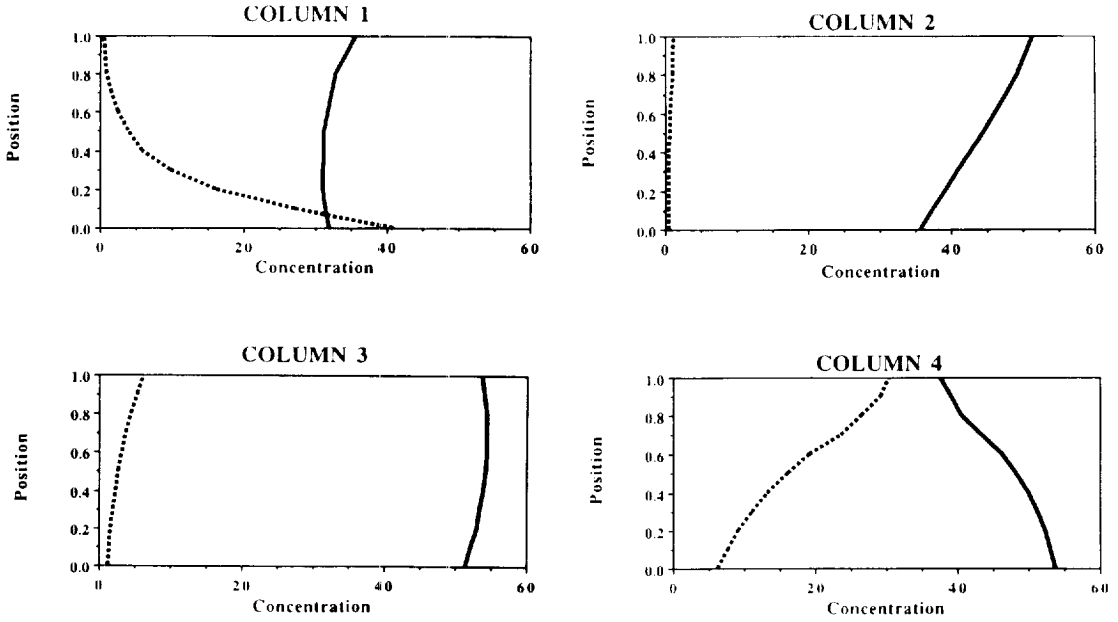

Fig. 2. Concentration profile of reactant and product in four columns. Fifteen per cent of outlet from top of column 2 is collected as product (solid line, product; dotted line, reactant; x-axis, concentration; y-axis, position in columns) (t_s = 120 s; σ_A = 1.2; σ_B = 0.3; % conversion = 96.7; % purity = 97.58).

a period equal to the switching time will be eventually reached. The concentration profiles for reactant and product shown in Figs 2–4 are plotted after at least six complete cycles through all four columns, which was sufficient to reach the periodic steady state.

The switching time used in the calculation for Fig. 2 is 120 s. All the calculations are made for low feed concentration ($\gamma_{Af} = 0.1$ and $\gamma_{Bf} = 0.0001$), so that the adsorption isotherms are approximately linear. The values of the other parameters, μ_i, δ_i and β are the same as for the equilibrium stage model calculations (Ray *et al.*, 1994). The conversion for the system is calculated from the ratio of total moles of product collected to the total moles of feed entering the feed column. For these parameter values, $\sigma_A = 1.2$ and $\sigma_B = 0.3$ and the model predicts 97.6% product purity and conversion of 96.7%.

Figure 3 shows the effect of decreasing the switching time and thereby the effect of increasing the hypothetical solid flow rate. In this figure, concentration profiles of reactant and product were obtained for the switching time of 80 s instead of 120 s, keeping all other parameter values unchanged. Under this operating condition, $\sigma_A = 1.8$ and $\sigma_B = 0.45$. In this case, the reactant moves relatively faster, as the pseudo-solids flow rate is higher, thereby shortening the reactant residence time in the column sufficiently that the conversion decreases. Much of the reactant reaches the product stream relatively faster and thus deteriorates the product purity. The appearance of more reactant than product in column 3 and column 4 is because less product is being formed by reaction due to shorter residence time. The conversion and product purity for this set of parameter values is 89.5 and 92.3%, respectively.

Figure 4 shows the calculated concentration profiles within columns of a five column configuration. In calculations made with this configuration, 15% of the exit fluid stream from column 2 is collected as product, similar to the earlier calculations. However, in this configuration there are three columns between the product take-off point and feed entry point instead of two. All parameter values were kept the same as Fig. 2. By adding one column, it is expected that conversion will improve substantially, as reactant residence time will be long enough for the reaction to be nearly complete. In the true countercurrent system, it was observed that product purity could be improved if the reactant were thoroughly stripped from the solids in a stripping section (Fish and Carr, 1989). Adding an additional column to the SCMCR is expected to have the same effect. Indeed, improvement in both conversion and product purity was calculated. For this configuration, the model predicts 99.3% product purity and conversion of 98.8%, respectively.

A direct comparison of these model predictions with experiments on MES hydrogenation in a five column SCMCR (Ray and Carr, 1995) is not possible because of differences between the reactor configurations. In the experimental investigation, all of the TMC product, which eluted ahead of MES, was removed at the exit of the feed column and the MES feed was advanced to the next column in line just before breakthrough. Because of the above-mentioned difficulties with numerical simulation of the steep concentration fronts that move through the columns in this mode of operation, it was necessary to modify the model configuration so that only 15% of the TMC containing flow was removed one column ahead of the feedpoint. This gave the gentler concen-

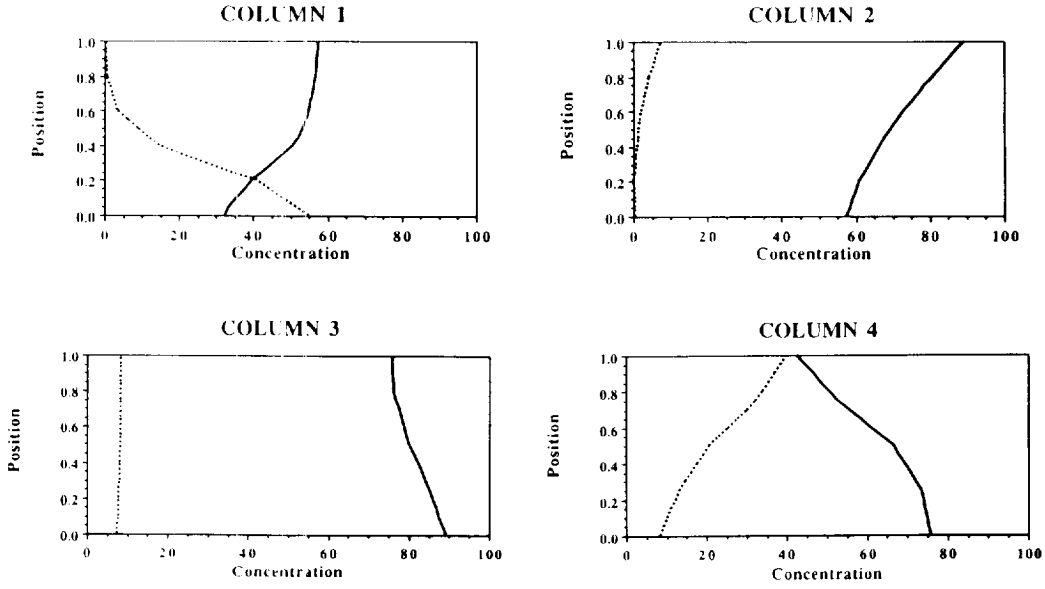

Fig. 3. Concentration profile of reactant and product in four columns. Fifteen per cent of outlet from top of column 2 is collected as product (solid line, product; dotted line, reactant; x-axis, concentration; y-axis, position in columns) ($t_s = 80$ s; $\sigma_A = 1.8$; $\sigma_B = 0.45$; % conversion = 89.5; % purity = 92.29).

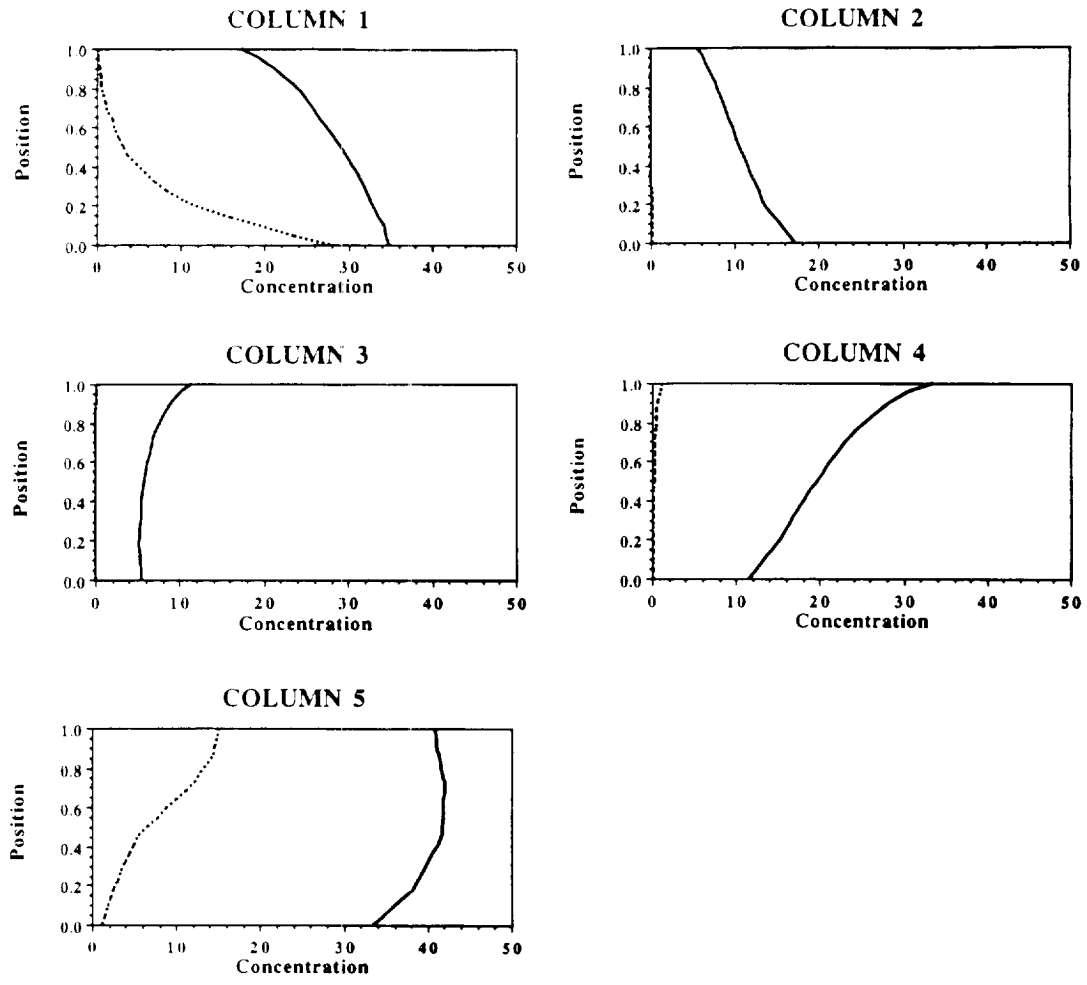

Fig. 4. Concentration profile of reactant and product in five columns. Fifteen per cent of outlet from top of column 2 is collected as product (solid line, product; dotted line, reactant; x-axis, concentration; y-axis, position in columns) (t_s = 120 s; σ_A = 1.2; σ_B = 0.3; % conversion = 98.8; % purity = 99.27).

Table 1. Comparison of reactor performance

	CMCR		SCMCR		
Reactor	Experiment†	Model†	Experiment‡	ES Model§	Model‖
Conversion, X_{MES}	0.88	0.97	0.83	0.97	0.98
Product purity, Y_{TMC}	0.95	1.00	0.96	0.98	0.99

† Fish and Carr (1989).
‡ Ray and Carr (1995).
§ Ray *et al.* (1994).
‖ This work.

tration gradients of Figs 2–4. It is interesting, nevertheless, to note that the predicted SCMCR-performance is very good. The five column SCMCR is predicted to give a conversion of 0.988, with 99.3% purity, which is to be compared with the best 463 K experimental results of 0.83 and 96%, respectively. In the countercurrent moving bed reactor (Fish and Carr, 1989), model predictions were also somewhat better than performance of the experimental unit.

Table 1 compares experimental results from both the CMCR and the SCMCR with model predictions. In all cases mesitylene hydrogenation was the test reaction. It can be seen that the model predictions of reactor performance are better than the experimental results. The principal cause of the discrepancy is that the models incorporate adsorption isotherms based upon a homogeneous surface, a surface with uniform adsorption energetics. The adsorbents used in the

experiments were either activated alumina or a mixture of alumina (the catalyst support) and Chromosorb 106. Analytical gas chromatography shows that MES peaks "tail" with these adsorbents, suggesting a distribution of adsorption energies which is not accounted for in the models. In the experiments this manifests itself as a "stickiness" that results in MES being distributed in the reactor in such a way that it contaminates the TMC product stream. Furthermore, MES that is strongly bound to the adsorbent is hindered from reaching the reactive sites on Pt and is purged from the reactor. Thus, the experimentally observed conversion is smaller than the model prediction. The adsorption equilibrium constants for the calculations were determined by pulse column chromatography and do not account for the effects of adsorption heterogeneity.

The discrepancy between the model predictions of this work and the experimental results cannot be attributed to inadequacies of the numerical method. Model predictions of reactor performance for both the single packed tower (Ray *et al.*, 1994) and the multiple column configuration reported here are remarkably similar. Rather, it is due to failure of the model to describe MES adsorption accurately. Nevertheless, the model calculations of concentration profiles in the columns, and how they change with operating conditions, lead to better understanding of SCMCR behavior.

CONCLUSION

A mathematical model based on the multiple column configuration of the simulated countercurrent moving bed chromatographic reactor (SCMCR) is developed. In this approach the transient partial differential equations governing reactor behavior are solved by the method of adaptive finite elements. This method combines the rapid convergence of the finite element method with the convenience associated with locating grid points where the solution has large gradients. Improved conversion and product purity were obtained for both four and five column configurations, over that of a fixed bed reactor. Results show that the concentration profiles in the individual columns are qualitatively quite similar to the predictions obtained from the equilibrium stage model of a single column multiple inlet and outlet configuration (Ray *et al.*, 1994).

Acknowledgement This work was supported by the Division of Chemical Sciences, Office of Basic Energy Sciences, U.S. Department of Energy, under grant number DE-AC02-76-ER02945.

NOTATION

A strongly adsorbed species; component A; reactant
B less strongly adsorbed species; component B; product
C fluid phase concentration; constant [eq. (27)]
e_i error bound of ith element
e_0 equidistribution of error
f forcing function
$\mathbf{F}$ load vector
F_i adsorption–desorption function
g gas
h mesh size
k rate constant
k_{ai} adsorption rate constant of component i
k_b backward surface reaction rate constant
k_{di} desorption rate constant of component i
k_f forward surface reaction rate constant
K adsorption equilibrium constant, K_A/K_B
K_i adsorption equilibrium constant of component i
K_r reaction equilibrium constant, k_f/k_b
L length of each reactor; linear operator [eq. (16)]
M number of segments
n solid phase concentration
N solid phase saturation concentration
R residual
R_i reaction function
$\mathbf{S}$ $\mathbf{U}^{-1}\mathbf{V}$
t time
t_s time interval between successive feed switching
$\mathbf{T}$ $\mathbf{U}^{-1}\mathbf{F}$
u_g carrier gas velocity
u_s velocity of solid phase
$\mathbf{U}$ mass or damping matrix
$\mathbf{V}$ stiffness matrix
X axial position

Greek letters

α stoichiometric coefficients
β ratio of pseudo-solid flow rate to carrier flow rate
γ dimensionless fluid phase concentration
δ dimensionless forward reaction rate
Δ $1 + \gamma_A + \gamma_B$
ε interparticle void fraction
φ basis function
λ dimensionless adsorption rate constant
ζ switching seed
μ phase ratio
σ relative carrying capacity
τ dimensionless time, t/t_s
υ dimensionless solid phase concentration
ξ dimensionless axial position

Suffix

0 initial state
a adsorption
ads adsorption
A component A
b backward
B component B
eq equilibrium
f forward
g gas
i component i; node location
j node location

k kth iteration
r reaction
s solid; switching

REFERENCES

Benner, R. E., Davis, H. T. and Scriven, L. E., 1987. An adaptive finite element method for steady and transient problems. *SIAM J. Sci. Stat. Comput.* **8** (4), 529.

Carr, R. W., 1993, Continuous Reaction Chromatography, in *Preparative and Production Scale Chromatography, Vol.* 61, *Chromatographic Science Series* (Edited by G. Ganetsos and P. E. Barker). Marcel Dekker, New York.

Davis, S. F. and Flaherty, J. E., 1987. An adaptive finite element method for initial value problems for partial differential equations. *SIAM J. Sci. Stat. Comput.* **3**, 6.

Egan, C. J. and Buss, W. C., 1959, Determination of the equilibrium constants for the hydrogenation of mesitylene. *J. Phys. Chem.* **63**, 1887.

Finlayson, B. A., 1980, *Nonlinear Analysis in Chemical Engineering*. McGraw-Hill, New York.

Fish, B. and Carr, R. W., 1989, Experimental study of the countercurrent moving bed chromatographic reactor. *Chem. Engng Sci.* **44**, 1773.

Gelinas, R. J., Doss, S. K. and Miller, K., 1981, The moving finite element method: applications to general partial differential equations with multiple large gradients. *J. Comput. Phys.* **40**, 202.

Petroulas, T., 1984, A countercurrent moving bed chromatographic reactor, Ph.D. thesis, University of Minnesota, Minneapolis, MN.

Ray, A. K. and Carr, R. W., 1995, Experimental study of a laboratory scale simulated countercurrent moving bed chromatographic reactor. *Chem. Engng Sci.* (in press).

Ray, A. K., Carr, R. W. and Aris, R., 1994, The simulated countercurrent moving bed chromatographic reactor: a novel reactor-separator. *Chem. Engg Sci.* **49** (4), 469.

Strang, G. and Fix, G. J., 1973, *An Analysis of the Finite Element Method*. Prentice-Hall, Englewood Cliffs, NJ.